Bol. Inst. Esp. Oceanogr. 15 (1-4). 1999: 39-60 **BOLETÍN** INSTITUTO ESPAÑOL DE OCEANOGRAFÍA
ISSN: 0074-0195

Transport and mixing simulation along the continental shelf edge using a Lagrangian approach

R. Miranda, P. C. Leitão, H. S. Coelho, H. Martins and R. R. Neves

Mechanical Engineering Department, Instituto Superior Técnico, Av. Rovisco Pais, 1096 Lisboa, Portugal

Received October 1997. Accepted April 1998.

ABSTRACT

This paper presents the coupling of a biochemical model with two different hydrodynamic models, a 1-D model (Coelho, 1996) and a 3-D model (Santos, 1995), corresponding to two successive work phases. In the first phase the 1-D hydrodynamic model was used to calibrate the biochemical model; the results of this phase made it possible to analyse temporal vertical profiles evolution. Both an Eulerian and a Lagrangian approach were used to transport biochemical properties. In the second phase, the 3-D hydrodynamic model was applied; this gave a regional-scale view of the processes involved. Biochemical properties transport was made with a Lagrangian approach, highlighting the origin of upwelled water. Goban Spur/La Chapelle field data collected during the Ocean Margin Exchange project (Anon., 1996) were used as initial and boundary conditions in hydrodynamic and biochemical models. Our main conclusion is that a 3-D particle-tracking model, coupled with a 3-D hydrodynamic model (with a proper turbulence closure model) and with a biochemical model, can be an excellent tool to quantify exchanges between the continental shelf and deep ocean.

Key words: Biochemical, particle-tracking, vertical turbulence and hydrodynamic models, Northeast Atlantic, deep ocean, continental shelf, primary production, Eulerian and Lagrangian transport.

RESUMEN

Transporte y simulación de mezcla a lo largo del borde de la plataforma continental mediante la aproximación langragiana

*Este trabajo presenta la comprobación de un modelo bioquímico a partir de dos modelos hidrodinámicos diferentes: un modelo 1D (Coelho, 1996) y un modelo 3D (Santos, 1995), correspondientes a dos fases de trabajo sucesivas. En la primera fase el modelo hidrodinámico 1D fue usado para calibrar el modelo biogeoquímico; los resultados de esta fase permitieron el análisis de la evolución de los perfiles temporales verticales. Se usaron tanto la aproximación euleriana como la lagrangiana para el transporte de las propiedades bioquímicas. En la segunda fase 3D se aplicó el modelo hidrodinámico, lo que permitió obtener una visión a escala regional de los procesos involucrados. El transporte de las propiedades bioquímicas fue realizado a partir de la aproximación lagrangiana, habiéndose destacado el origen del agua procedente de afloramientos (*upwelling*). Los datos obtenidos en Goban Spur/La Chapelle durante el Ocean Margin Exchange Project (Anon., 1996) fueron usados para definir las condiciones iniciales y de contorno para los modelos bioquímicos e hidrodinámicos. Nuestra principal conclusión es que el modelo 3D de seguimiento de la dinámica de partículas, junto con el modelo hidrodinámico 3D (con un modelo de turbulencia cerrado apropiado) y con un modelo bioquímico, puede ser una excelente herramienta para cuantificar intercambios entre la plataforma continental y el océano abierto.*

Palabras clave: *Bioquímica, transporte de partículas, turbulencia vertical y modelos hidrodinámicos, Atlántico nororiental, océano profundo, plataforma continental, producción primaria, aproximaciones euleriana y lagrangiana.*

INTRODUCTION

Under real environmental conditions, algae undergo large incident light variations within time scales smaller than their reproduction time scale. In the upper ocean layer, algae are subjected to considerable vertical motion, mainly due to vertical transport associated with turbulence mixing. During this motion, algae are exposed to a variable incident light field that decreases exponentially with depth. Understanding the relationship between physical environmental conditions and ecosystem dynamics is still a very complex matter. In the past, the establishment of empirical correlations was the method most often used. The problem is that a good correlation does not necessarily mean that a cause-effect relationship exists. On the other hand, there is no limit for the number of correlations that one might establish, making it impossible to decide whether they are coincidental or not.

The number of interactions in the ocean is very large. Nevertheless, there are sequences that always occur. A good example is the mixed-stratified-mixed sequence that occurs in the upper ocean in different time and spatial scales -e.g. daily cycle and seasonal cycles. This sequence is controlled by turbulence intensity, which depends upon production and destruction terms. The major production terms are wind stress acting on the sea surface, buoyancy losses across the surface, and dynamic instabilities in the base of the mixed layer, often associated with internal waves. The destruction terms are solar radiation, which is vertically distributed by the water column, and the buoyancy gain across the sea surface. The mixed-stratified sequence enhances primary production, mainly through diatoms (Cushing, 1989), which are either ingested by mesozooplankton or sink and are eaten by benthic invertebrates, being at the base of the food chain. Thus, diatoms also constitute the support for the fish stocks that are economically important. The mechanism that produces the mixed-stratified sequence enables us to understand how physical processes control biological production, and ultimately the size of fish stocks.

Available data show that in several cases, variability in stocks is much more affected by physical processes than by management practices. If it were possible to predict variations in stocks based on atmospheric and ocean climate, it would be a powerful tool for fisheries management and environmental impact studies (Mann, 1993).

In the present paper, we use a one-dimensional, vertical physical model, with a very simple turbulence closure, coupled with transport models –Lagrangian and Eulerian– solving biogeochemical equations. Some simple cases are reproduced, enhancing the importance of atmospheric forcing on the vertical mixing. Consequences of this forcing for biology are also quantified.

Results of primary production biomass over an area including the Bay of Biscay, La Chapelle Bank and Goban Spur (43°-53° N and 20°-0° W) are presented. These results show that a 3-D particle-tracking model coupled with a 3-D hydrodynamic model (with a proper turbulence closure model) and a biogeochemical model can be an excellent tool to quantify exchanges between the continental shelf and deep ocean.

MATERIALS AND METHODS

Physical model

Previous work on the simulation of the diurnal temperature cycle within the scope of the Long-Term Upper Ocean Study (LOTUS) in the Sargasso Sea, and the seasonal cycle of temperature off the Iberian coast, showed that two different models based on the Gaspar, Grégoris and Lefevre (1990) one-equation turbulence closure and on the quasi-equilibrium version of the 2.5-level Mellor and Yamada closure scheme (Galperin *et al.*, 1988), respectively, produce similar results. Therefore, and for simplicity's sake, the one-equation closure scheme was adopted for the present paper.

The unidimensional forms of the balance equations for temperature, salt and momentum are:

$$\frac{\partial \overline{T}}{\partial t} = \frac{F_{sol}}{\rho_0 C_p}\frac{\partial I}{\partial z} - \frac{\partial \overline{T'w'}}{\partial z}$$

$$\frac{\partial \overline{S}}{\partial t} = \frac{\partial \overline{S'w'}}{\partial z}$$

$$\frac{\partial \overline{U}_H}{\partial t} = -fk \times \overline{U}_H - \frac{\partial \overline{u_H'w'}}{\partial z}$$

where T, S, U_H and w are the mean temperature, salinity, horizontal velocity and vertical velocity of the water column, respectively. $\overline{X}$ denotes mean

quantities and x' denotes fluctuations around the mean. ρ_0 and C_p are the reference density and the specific heat of the seawater, respectively, F_{sol} is the solar irradiance absorbed at sea surface. I(z) is the fraction of F_{sol} that penetrates to the depth z. f is the Coriolis parameter and k the vertical unit vector.

The surface boundary conditions are

$$-\rho_0 C_p \overline{T'w'}(0) = F_{nsol} = H + LE + F_{ir}$$

$$-\rho_0 C_p \overline{S'w'}(0) = E - P$$

$$-\rho_0 \overline{u_H'w'}(0) = \tau$$

where F_{nsol} stands for the surface latent heat (LE), plus the sensible heat fluxes (H), plus the long-wave radiation (F_{ir}). E and P are the evaporation and the precipitation rates, respectively, and τ is the surface wind stress. Heat fluxes are positive downwards. These surface fluxes were computed from observational atmospheric data collected using the Large and Pond (1981, 1982) method.

Turbulence model

The vertical turbulence fluxes are parameterised using the turbulent viscosity/diffusivity concept:

$$-\overline{T'w'} = K_h \frac{\partial \overline{T}}{\partial z}$$

$$-\overline{S'w'} = K_s \frac{\partial \overline{S}}{\partial z}$$

$$-\overline{u_H'w'} = K_m \frac{\partial \overline{U}_H}{\partial z}$$

Viscosity and diffusivities are related with length and velocity scales according to:

$$K_m = c_k l_k \overline{e}^{1/2} \qquad K_s = K_h = K_m / P_{rt}$$

where c_k is a constant to determine, l_k is the mixing length, $\overline{e}$ is the turbulent kinetic energy (TKE) $e = 0.5\ (u'^2 + v'^2 + w'^2)$. P_{rt} is the turbulent Prandtl, assumed to be 1 (this choice is supported by some laboratory experiments and oceanic observations, cf. Mellor and Yamada, 1982; Gregg *et al.*, 1985).

To close the system, TKE is determined from its balance equation

$$\frac{\partial \overline{e}}{\partial t} = -\frac{\partial}{\partial z}\left(\overline{e'w'} + \frac{\overline{p'w'}}{\rho_0}\right) - \overline{u_H'w'}\frac{\partial \overline{U}_H}{\partial z} + \overline{b'w'} - \varepsilon$$

being p the pressure, ε the dissipation rate of TKE, and b the buoyancy $b = g\,\frac{(\rho_0 - \rho)}{\rho_0}$, where g is gravity. Density ρ is determined by a state equation:

$$\rho = \rho_0[1 - \alpha(T - T_0) + \beta(S - S_0)]$$

where 0 refers to a reference state and α e β are, respectively, the coefficients of thermal expansion and haline contraction, calculated according to Bryan and Cox (1972).

For the diffusivity of density we have

$$K_\rho = K_m / P_{rt}$$

The turbulent diffusivity concept is also used to parameterise the vertical flux of turbulent kinetic energy

$$-\left(\overline{ew'} + \frac{\overline{p'w'}}{\rho_0}\right) = K_e \frac{\partial \overline{e}}{\partial z}$$

with the usual assumption that $K_e = K_m$. The dissipation rate is parameterised as follows:

$$\varepsilon = \frac{c_\varepsilon \overline{e}^{3/2}}{l_\varepsilon}$$

being c_ε a constant to be determined and l_ε the length scale for dissipation.

Length scales

The major difficulty of models that parameterise the turbulent viscosity based on velocity and length scales is the determination of such scales, especially the length scale. In this model, very simple definitions of the length scales are used, avoiding a large number of coefficients and leading to very reasonable results, like those obtained by Bougeault and Lacarrère (1989). The mixing length definitions are

$$l_\varepsilon = (l_u\, l_d)^{1/2}$$

$$l_k = \min\,(l_u, l_d)$$

being l_k and l_ε the length scales for mixing and dissipation, respectively, and l_u (mixing length upward) and l_d (mixing length downward) were obtained according to Bougeault and André (1986)

$$\frac{g}{\rho_0}\int_z^{z+l_u} [\overline{\rho}(z) - \overline{\rho}(z')]\,dz' = \overline{e}(z)$$

$$\int_{z}^{z-l_d} [\overline{\rho}(z) - \overline{\rho}(z')]dz' = \overline{e}(z)$$

Model constants

Two constants are to be determined, c_k and c_ε. From laboratory experiments, Bougeault and Lacarrère (1989) deduced that $c_\varepsilon = 0.7$ is an adequate value for simulations. The choice of c_k is more difficult to justify from observations. Based on the definition of the mixing efficiency coefficient, $\gamma = \frac{R_f}{1 - R_f}$, where R_f is the Richardson flux number, $R_f = \frac{\overline{b'w'}}{\overline{u_H'w'}\,\frac{\partial \overline{U}_H}{\partial z}}$ it is possible to deduce that $c_k = 0.15\ c_\varepsilon$ (for details see Gaspar, Grégoris and Lefevre, 1990). The critical Richardson number associated with this value is 0.23.

Diffusion below the mixed layer

To avoid unrealistically small diffusion and dissipation rates in the pycnocline, Gaspar, Grégoris and Lefevre (1990) suggested that a minimal value for TKE should be imposed. To match results, $\overline{e}_{min}$ is set equal to $10^{-6} m^2 s^{-2}$. This represents a very simple solution to obtain realistic diffusion rates in the thermocline. Gaspar, Grégoris and Lefevre (1990) suggested that better results could probably be obtained by a $\overline{e}_{min}$ parameterisation function of internal wave activity and surface forcing. For the present paper, we choose the same value for $\overline{e}_{min}$.

The pelagic biochemical model

This pelagic ecological model uses a trophic structure approach, where energy flows from the autotrophic to the heterotrophic producers. In real-life situations, however, this is not the case, and instead of occupying clear trophic positions, most creatures feed on almost everything suitable in size and accessible to their mode of feeding (Isaacs, 1973).

Our aim is to quantify the new production, a most topical theme, because if the day models are able to calculate it, we shall be closer to knowing the fate of the greenhouse gas carbon dioxide. To compute (new) production we are interested in an ecosystem level, and it will suffice that we understand and modulate the processes relevant to it. Sometimes a particular population has a prominent role in the community behaviour (Mann, 1988). In these cases, an ecosystem approach may lead to poor results.

Each ecosystem has its own dynamics and behaves like an entity with characteristics of its own; i.e. we cannot infer the response of an ecosystem from the knowledge of the response of each population. (More mathematically, we can state that due to the non-linearity of populations' intra- and interrelations, the results of separate population studies are not summable.) If a population shows a periodic fluctuation, this does not necessarily mean that a forcing function with the same periodicity is to be found.

This discussion leads to the conclusion that trophic levels like 'herbivore' or 'carnivore' are abstractions of an ecosystem-level approach, not concrete units that one can assign to groups of taxa (Odum, 1971). We should focus on whether this ecosystem point of view can lead to good model results, not expecting the model to give population-level responses.

The present biochemical model simulates nitrogen (three inorganic forms –ammonia, nitrate, and nitrite -and three organic forms– refractory and non-refractory dissolved organic nitrogen and particulate organic nitrogen), primary and secondary production. There is a system of 8 coupled partial differential equations, one for each variable, governing the vertical and temporal distribution of a non-conservative property

$$\frac{\partial B}{\partial t} + w\frac{\partial B}{\partial z} = \frac{\partial}{\partial B}\left(K\frac{\partial B}{\partial B}\right) + S_B$$

where B is a non-conservative property, z the vertical position, w is the vertical velocity, K the diffusion coefficient (output of the hydrodynamic model) and S_B the sink-and-source term. The following sections present the S_B term for each one of the properties.

Secondary producers

Secondary producers' dynamics are represented by

$$\frac{dZ}{dt} = (g_z - r_z - m_z)Z - G_z$$

where Z stands for the concentration of secondary producers, g_z the net growth rate, r_z the rate of biomass loss by respiration and excretion, m_z the non-predatory mortality rate and G_z the predatory mortality.

The net growth tax, g_z is obtained from

$$g_z = g_{max}\ (T_{ref})\ \psi(T)\ \left(1 - e^{-\Lambda(F - F_o)}\right)$$

where $g_{max}(T)$ is the maximum growth rate at a reference temperature with no food constraints (Ivlev, 1945, adapted by Parsons, Lebrasseur and Fulton, 1967). The symbol Λ is the Ivlev grazing constant. F_o is the minimal primary producers' concentration for the existence of grazing. F is the concentration of primary producers.

The effect of temperature on growth, $\psi(T)$, as proposed by Thornton and Lessen (1978), is given by

$$\psi(T) = K_A(T)\ K_B(T)$$

where

$$K_A(T) = \frac{k_1 e^{\gamma_1 (T - T_{min})}}{1 + k_1[e^{\gamma_1 (T - T_{min})} - 1]};$$

$$\gamma_1 = \frac{1}{[T_{opt(1)} - T_{min}]}\ ln\left[\frac{k_2(1 - k_1)}{k_1(1 - k_2)}\right]$$

$$K_B(T) = \frac{k_4 e^{\gamma_2 (T_{max} - T)}}{1 + k_4[e^{\gamma_2 (T_{max} - T)} - 1]};$$

$$\gamma_2 = \frac{1}{[T_{max} - T_{opt(2)}]}\ ln\left[\frac{k_3(1 - k_4)}{k_4(1 - k_3)}\right]$$

$T_{opt(1)}$ is the minimal value of the optimal interval to growth, being $T_{opt(2)}$ the maximal. T_{min} is the minimum tolerable temperature; at this temperature, the growth rate is zero. T_{max} is the maximum tolerable temperature. The remaining constants are used to control the shape of the response curve.

Respiration and non-predatory mortality of the zooplankton are considered functions of temperature, being treated as the variable

$$r_z + m_z = d_z(T_{ref})\ \psi_r(T)$$

where $d_z\ (T_{ref})$ is the rate of carbon consumption by respiration and non-predatory mortality of secondary producers at the reference temperature T_{ref}, while $\psi_r(T)$ stands for the influence of temperature.

The predatory mortality, G_z, depends on the heterotrophic producers' concentration

$$G_z = e_z\ Z$$

where e_z represents the predatory mortality (Scavia *et al.*, 1976; Scavia, 1980).

Primary producers

Primary production sink-and-source terms are

$$\frac{dF}{dt} = (\mu - r - e_x - s - m)F - G$$

where F is the autotrophic producers' concentration, μ the gross growth rate, r the respiration rate, e_x the excretion rate, m the non-grazing mortality and G the rate of mortality due to grazing.

The gross rate of phytoplankton growth, μ, is given by

$$\mu = \mu_{max}(T_{ref})\ \psi(T)\ \psi(L)\ min(\psi(P), \psi(N))$$

where $\mu_{max}(T_{ref})$ stands for the maximum growth rate at a reference temperature T_{ref}, usually 20° C. The light intensity must be optimal and there should not be lack of nutrients. The function $\psi(T)$ is presented in the previous section.

A Michaelis-Menten formulation was assumed for the nitrogen-limiting factor

$$\psi(N) = \frac{NH_4^+ + NO_3^-}{K_N NH_4^+ + NO_3^-}$$

where k_N is a constant that represents the substrate concentration at which $\psi(N) = 1/2$.

$\psi(N) = \dfrac{[NH_3 + NO_3]}{kN + [NH_3 + NO_3]}$ is the useful concentration of inorganic dissolved nitrogen (ammonia and nitrate).

The light-intensity limiting factor is modulated according to Steele (1962),

$$\psi(L) = \frac{I(z)}{I_s}\ e^{\left(1 - \frac{I(Z)}{I_s}\right)}$$

where I_s stands for the best light intensity for photosynthesis and z for the vertical position.

I(z) is given by

$$I(z) = I_0 \exp(-k(Part)z)$$

where I_0 is the effective solar radiation at the water surface and K_d is the light extinction factor (function of particulate matter in suspension, including the phytoplankton concentration).

The light-attenuation factor, k_d, is obtained according to Parsons, Takahashi and Hargrave (1995)

$$k(\text{Part}) = k_R\, \theta^{(\text{Part} - \text{Part}_R)}$$

where Ch is the chlorophyll concentration.

Integrating $\psi(L)$ vertically, we obtain

$$\psi(L) = \frac{I_0}{I_s k_d (z_1 - z_0)} F(z) \exp\left(1 - \frac{I_0}{I_s k_d (z_1 - z_0)} F(z)\right)$$

The respiration may be divided into dark respiration and photorespiration, $r = r_e + r_p$ being r_e the dark respiration and r_p the photorespiration.

For the dark respiration

$$r_e = 0.0175 e^{0.069T}$$

where k_{er} is the phytoplankton endogenous respiration constant. The photorespiration is proportional to the gross photosynthetic rate

$$r_p = k_p \mu$$

being k_p the proportionality factor.

The excretion rate, e_x, is calculated taking in account that its importance is bigger when the solar radiation is either very low or very high (Collins, 1980), with

$$e_x = k_e\, (1 - \psi(L))\, \mu$$

where k_e is a non-dimensional constant.

The non-grazing mortality m, is, according to a modified Michaelis-Menten formulation proposed by Rodgers and Salisbury (1981), proportional to the biomass of phytoplankton and inversely proportional to the gross growing rate μ

$$m(T_{ref}) = m_{max}(T_{ref}) \left(\frac{F/\mu}{k_m + F/\mu}\right)$$

where k_m is a mortality semi-saturation constant and $m_{max}(T_{ref})$ is the maximum mortality rate at a reference temperature.

The rate of mortality due to grazing, G, is given by

$$G = C_g\, Z$$

where, as mentioned above, g_z and Z are, respectively, the net growth rate and the concentration of the heterotrophic producers. E is the heterotrophic assimilation efficiency.

Nitrogen dynamics

The concentration of the various forms of nitrogen present in the water column is calculated by solving a system of 6 equations, one for each form of nitrogen considered. The system is shown below, and the equations stand for the evolution of ammonia (NH_4^+), nitrate (NO_3^-), nitrite (NO_3^-), particulate organic nitrogen (PON), refractory dissolved organic nitrogen (DONr) and non-refractory dissolved organic nitrogen (DONnr):

$$S_{NH_4^+} = f_{1N}(e_{NF} + e_{NZ}) - \Phi_{NH_4^+} - k_{2N}NH_4^+ + \\ + k_{1Nnr}\text{DONnr} + k_{1Nr}\text{DONr} + k_{det}\text{PON}f_2$$

$$S_{NO_2^-} = k_{2N}NH_4^+ - k_{2N}NO_2^-$$

$$S_{NO_3^-} = k_{2N}NO_2^- - \Phi_{NO_3^-} - k_{3N}NO_3^-$$

$$S_{PON} = (1 - f_D)(1 - f_{1N})(e_{NF} + e_{NZ}) - k_{det}\text{PON} + \\ + \underbrace{mF\alpha_{N:C}}_{\substack{\text{phytoplankton}\\ \text{mortality}}} + \underbrace{g_z Z \alpha_{NZ}\left(\frac{1-E}{E}\right)}_{\substack{\text{non-assimilated}\\ \text{phytoplankton}}} + \underbrace{g_z Z(\alpha_{N:C} - \alpha_{NZ})}_{\substack{\text{stoichiometric food web}\\ \text{losses}}}$$

$$S_{DONnr} = f_D\, (1 - f_{1N})(e_{NF} + e_{NZ}) - k_{1N}\text{DONnr}$$

$$S_{DON} = k_{det}\text{PON}(1 - f_2) - k_{1Nr}\text{DONr}$$

where f_{1N} is the inorganic fraction of the plankton excretions, f_D is the inorganic plankton excretions dissolved fraction, e_{NF} is the excretion rate of soluble nitrogen compounds by primary producers, and e_{NZ} is the same for the secondary producers (see below). K_{1N} is the rate of hydrolysis of DON, k_{2N} the nitrification rate, k_{3N} the denitrification rate and k_{det} is the rate of the particulate nitrogen organic compounds' decomposition.

Nitrogen is consumed preferentially in the form of ammonia; only in its absence is nitrate used up. The photosynthetic assimilation rates for each of them are

$$\Phi_{NH_4^+} = \beta_{NH_4^+}\, \alpha_{N:C} \mu F$$

and

$$\Phi_{NO_3^-} = (1 - \beta_{NH_4^+}) \alpha_{N:C} \mu F$$

where $\beta_{NH_4^+}$ is the ammonia preference factor and $\alpha_{N:C}$ is the nitrogen fraction in the phytoplankton composition, given by

$$\beta_{NH_4^+} = \frac{NH_4^+ NO_3^-}{(k_N + NH_4^+)(k_N + NO_3^-)} + \\ + \frac{NH_4^+ k_N}{(NH_4^+ + NO_3^-)(k_N + NO_3^-)}$$

where k_N is the nitrogen semi-saturation constant given above.

The DON hydrolysis rate is given by

$$K_{1N} = M_{DON}(T_{ref})\theta_{DON}^{(T - T_{ref})}$$

where $M_{DON}(T_{ref})$ is the reference decomposition rate and is the temperature coefficient.

The nitrification rate, k_{2N}, is given by

$$k_{2N} = M(T_{ref})\theta^{(T - T_{ref})}\left(\frac{O_2}{k_n + O_2}\right)$$

where $M(T_{ref})$ is the reference nitrification rate, θ is the temperature coefficient, k_n is the nitrification semi-saturation constant and O_2 is the oxygen concentration.

The denitrification rate, k_{3N}, is given by

$$k_{3N} = M_{NO_3^-}(T_{ref})\theta_{NO_3^-}^{(T - T_{ref})}\left(\frac{k_d}{k_d + O_2}\right)$$

where $M_{NO_3^-}(T_{ref})$ is the reference rate, $\theta_{NO_3^-}$ is the temperature coefficient and k_d is the denitrification semi-saturation constant.

The particulate nitrogen organic compound decomposition rate is given by

$$K_{det} = M_{PON}(T_{ref})\theta_{PON}^{(T - T_{ref})}$$

where $M_{PON}(T_{ref})$ and θ_{PON} are, respectively, the reference rate and temperature coefficient.

e_{NF} is the excretion of soluble nitrogen compounds by primary producers, given by

$$e_{NF} = \alpha_N(r + e_x)F$$

and e_{NZ} the excretion of soluble nitrogen compounds by secondary producers, given by

$$e_{NF} = \alpha_{NZ}(r_z + m_z)Z$$

The Lagrangian transport model

Former Lagrangian models used particle-tracking approaches, where a particle represented a water mass whose trajectory is tracked for a better understanding of local transport mechanisms. In these models, the basic properties of particles used are their spatial co-ordinates and origin. Recently, more sophisticated versions were developed, especially dispersion models of passive tracers, aiming at the study of their impact on marine ecosystems. In these models, the variables associated with each particle include the amount of a certain property which is transported (e.g. coliforms, temperature, phytoplankton), and other basic properties, including particle volume, settling velocity, mixing length, and random velocity.

In the early 1980s the dispersion models using the particle-tracking technique became a generalised environmental management tool. Their most common application was for the simulation of property transport with source points, e.g. powerplant cooling water or wastewater discharges (Bork and Maier-Reimer, 1978; Monteiro, Neves and Sousa, 1992; Neves and Martins, 1996). In these cases, strong horizontal (and often vertical) gradients are present, and the size of plumes is much smaller than the size of the modelling area.

The computational speed and availability of modern computers is increasing all the time, allowing the modeller to simulate more and more complex mechanisms. Particle tracking models are currently used to simulate a wide variety of complex processes, including: sediment transport (Kelsey *et al.,* 1994), oil spreading (Shiau, 1991; Mansur and Price, 1992), and phytoplankton growth dynamics (Woods and Onken, 1982; Dippner, 1993; Rodrigues, Neves and Miranda, 1996).

This type of model does not present numerical diffusion problems due to the calculation of advective transport, but the calculation of diffusion is much more difficult than in Eulerian models. In general, diffusion is computed by adding a random component to the mean velocity calculated by the hydrodynamic model. This is a reasonable approach to simulate the effect of eddies larger than the particle. Eddies smaller than the particle do not cause a random movement of the particle, but instead mix the particle with the surrounding water, increasing its volume and modifying its mass

and concentration, according to the characteristics of the water entrained in the particle.

The 3-D particle-tracking model used in the present study was initially developed to be coupled with a 2-D hydrodynamic depth-integrated model (Neves, 1985). It was used as a calibration tool for the hydrodynamic model. In a second stage, the model was extended to simulate more complex mechanisms: wastewater discharges, localised sediment emission (e.g. rivers, dredged products), the trajectory of oil spills, and to calculate residence times. In a third stage, the model was generalised to be coupled with the 2-D or 3-D Cartesian or sigma-hydrodynamic models (Leitão, 1997).

In this model, the particles have six main properties: spatial co-ordinates (x, y, z), random horizontal/vertical velocities, time to perform the random movement, settling velocity, mass, and volume. For each one of these properties, evolution equations must be solved. The mass can be an array of properties (e.g. nitrate, phytoplankton, zooplankton, ammonia, oxygen). The last five properties are optional. If not considered, only the mean movement of the particles is studied.

Particle movement

The major factor responsible for particle movement is generally the mean velocity. The spatial co-ordinates are given by the definition of velocity

$$\frac{dx_i}{dt} = u_i(x_i, t)$$

$$u_i = \overline{u}_i + u_i'$$

where $\overline{u}_i$ is the mean velocity (hydrodynamic model) and u_i' the random velocity (turbulent model).

Turbulent transport

Turbulent transport is responsible for dispersion. The effect of eddies on the particles depends on the ratio between the eddy's sixe and the size of the particles. Eddies larger then the particle cause a random movement of the particle. Eddies smaller than the particle cause entrainment of matter into the particle, increasing its volume and its mass according to the environmental concentration.

Random movement is calculated following the Allen's procedure (1982). Random displacement is calculated using the mixing length and the standard deviation of the turbulent velocity component, as given by the turbulence closure of the hydrodynamic model. The particles maintain that velocity during the time needed to perform the random movement, which is dependent on the local turbulent mixing length.

In the present paper, only vertical diffusion was considered. The mixing length and turbulent velocity standard deviation was computed using the 1-D turbulence model described above. To obtain a better description of the tracers' trajectory, two types of mixing length values were used: mixing length upwards (l_u) and downwards (l_d). Basically, this makes it possible to simulate strong vertical anisotropy of the turbulent flow in the ocean, especially near the mixed-layer bottom. Each random movement can be equal to l_u if the random velocity is positive (upwards) or equal to l_d (downwards) if the opposite is true.

The increase in volume is associated with small-scale turbulence, and it is reasonable to assume that it is isotropic. Under these conditions, small particles do keep their initial form and the increase in volume is a function of the volume itself. However, for simplicity's sake, tracers with constant volume were assumed in this paper.

Properties evolution

The Lagrangian transport model was also coupled with the biochemical model described above. This model simulates the sink-and-source terms of the following properties: nitrogen (three inorganic forms and three organic forms), primary and secondary production. The Lagrangian transport model solves the equation

$$\frac{dB}{dt} = \frac{\partial}{\partial x_i}\left(K_{ij}\frac{\partial B}{\partial x_j}\right) + S_B$$

where B is a non-conservative property. The first term on the right side of the equation represents the water entrained in the particle forced by eddies smaller than the particle. This term was assumed to be equal to zero in the present paper, because the model work was centred only on the spring bloom. In the future, the succession spring bloom–autumn

bloom will be simulated and at that time this term must be considered, since the mixed layer grows in autumn. The particle must be able to incorporate nitrates by diffusion when it moves to greater depths (large environmental concentrations of nitrates) because the particle nitrates were consumed during the spring bloom. The second term on the right side of the equation, S_B, is the sink-and-source term computed by the biogeochemical model. It is important to remember that this model solves only sink-and-source terms of water masses, and was developed with the aim of being coupled with any kind of transport model: Eulerian or Lagrangian.

RESULTS

Although the previous discussion of the ecological model focused on biogeochemical processes, the impact of physical environment is by no means negligible (Huthnance *et al.*, 1993). The advective transport of nutrients (e.g. in strong upwelling regions), turbulent mixing (e. g. in the mixed layer), and the amount of light available for photosynthesis are good examples of physical processes that may have an overwhelming influence on an ecosystem's productivity.

The Goban Spure/La Chapelle study area is no exception, which is why we coupled a biochemical model with two different hydrodynamic models, a 1-D (Coelho, 1996) and a 3-D model (Santos, 1995), corresponding to two successive work phases. In the first phase the 1-D hydrodynamic model was used to calibrate the biochemical model; the results of this phase made possible the temporal evolution analysis of vertical profiles. In the second phase, we applied the 3-D hydrodynamic model, which gave us a regional-scale view of the processes involved.

Goban Spur/La Chapelle field data collected during the 'Ocean Margin Exchange' project (Anon., 1996) were to define initial and boundary conditions in hydrodynamic and biogeochemical models.

Biochemical 1-D hydrodynamic results

The 1-D hydrodynamic model output results required for a biochemical model when a Eulerian approach is used in the transport of biochemical properties are: vertical profiles of temperature, salinity and vertical diffusion coefficients. On the other

Table I. Rates and constant default values are defined on a per-hour basis. They could also be defined in terms of days or seconds

Non-specific				
Description	Name	Units	Range	Default
Time step between 2 water quality calls	–	h	–	1
Nitrogen half-saturation constant	k_N	mgN/l	–	0.014
Phytoplankton nutrient regeneration half saturation rate	k_f	mgC/l	–	0.0
Phytoplankton ratio between nitrogen and carbon	$\alpha_{N:C}$	mgN/mgC	–	0.18
Soluble inorganic fraction of the plankton excretions	f_1	–	0.25-0.5	0.5
Nitrogen				
Description	Name	Units	Range	Default
Zooplankton ratio between nitrogen and carbon	α_{NZ}	mgN/mgC	–	0.15
Reference ammonia mineralization rate	M_{ON}	l/day	–	0.1
Reference denitrification rate	$M_{NO_3^-}$	l/day	–	0.01
Reference nitrification rate	$M_{NH_4^+}$	l/day	–	0.0
Nitrogen mineralisation temperature coefficient	θ_{ON}	–	–	1.02
Reference particulate matter decomposition rate	M_{PON}	l/day		0.0
Denitrification temperature coefficient	$\theta_{NO_3^-}$	–	–	1.045
Denitrification semi-saturation constant	k_d	mgO_2/l	–	0.1
Phytoplankton				
Description	Name	Units	Range	Default
Maximum phytoplankton growth rate	μ_{max}	l/h	1.0-2.7	2.4/24
Phytoplankton maximum mortality	m_{max}	mgC/l h	–	0.03/24
Assimilation efficiency of the phytoplankton by the zooplankton	E	–	0.5-0.75	0.6
Minimum temperature of the optimal interval for phytoplankton growth	$T_{opt(1)}$	°C	–	25.0

Table I (continued)

Phytoplankton				
Description	Name	Units	Range	Default
Maximum temperature of the optimal interval for phytoplankton growth	$T_{opt(2)}$	°C	–	26.5
Minimum tolerable temperature of the interval for phytoplankton growth	T_{min}	°C	–	4.0
Maximum tolerable temperature of the interval for phytoplankton growth	T_{max}	°C	–	37.0
Constant to control temperature response curve shape	k_1	–	–	0.05
Constant to control temperature response curve shape	k_2	–	–	0.98
Constant to control temperature response curve shape	k_3	–	–	0.98
Constant to control temperature response curve shape	k_4	–	–	0.02
Mortality half-saturation rate	k_m	mgC/l h		0.3/24
Fraction of actual photosynthesis that is oxidised by photorespiration	k_p	–	–	0.018
Excretion constant	k_e	–	–	0.08
Phytoplankton endogenous respiration constant	k_{er}	l/h	–	7.29E-4
Zooplankton				
Description	Name	Units	Range	Default
Maximum zooplankton growth rate	g_{max}	l/h	–	0.16/24
Minimum temperature of the optimal interval for the zooplankton growth	$T_{opt(1)}$	°C	–	24.8
Maximum temperature of the optimal interval for the zooplankton growth	$T_{opt(2)}$	°C	–	25.1
Minimum tolerable temperature of the interval for the zooplankton growth	T_{min}	°C	–	5.0

Table I (continued)

Zooplankton				
Description	Name	Units	Range	Default
Maximum tolerable temperature of the interval for the phytoplankton growth	T_{max}	°C	–	35.0
Constant to control temperature response curve shape	k_1	–	–	0.05
Constant to control temperature response curve shape	k_2	–	–	0.98
Constant to control temperature response curve shape	k_3	–	–	0.98
Constant to control temperature response curve shape	k_4	–	–	0.02
Minimum phytoplankton concentration for the existence of grazing	F_0	mgC/l		0.0045
Ivlev grazing constant	Λ	–	–	16.0
Predatory mortality rate	e_z	1/h	–	3.21 E4
Rate of consumption of Carbon by respiration and non-predatory mortality at the reference temperature	d_z	1/h	2.08 E4-0.0052	0.0015

hand, if the Lagrangian approach is used, the required properties are the vertical profiles of temperature, salinity, mixing lengths (upward and downward) and turbulent velocity standard deviation.

The model was forced using atmospheric data and sea-surface temperature from the K_1 buoy at 48.7° N, 12.4° W over the Goban Spur (figure 1). Data were made available by the UK Meteorological Office via the British Oceanographic Data Centre (BODC). Assuming that horizontal gradients are small, we can ignore lateral advection and, therefore, a 1-D hydrodynamic model is applicable. Water surface temperature model validation is shown in figure 2. For further discussion of the 1-D hydrodynamic model Goban Spur simulation, see Huthnance *et al.* (submitted).

Eulerian approach

Figure 3 shows the water-column temperature evolution, calculated with the 1-D hydrodynamic

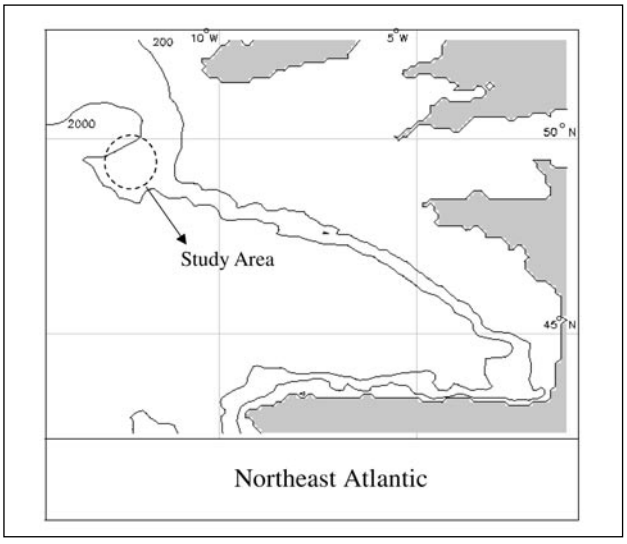

Figure 1. Study area

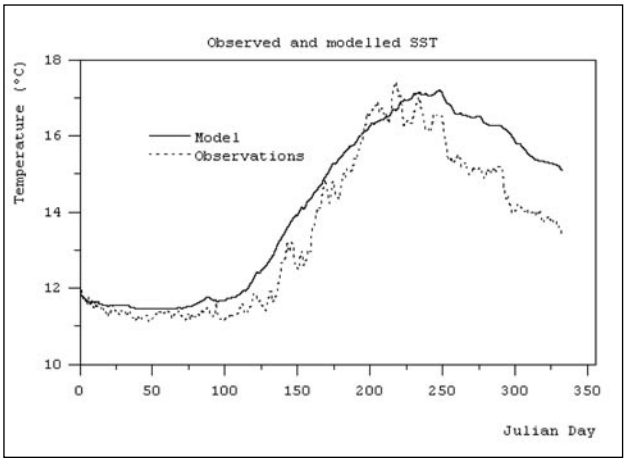

Figure 2. 1-D hydrodynamic model and field data water surface temperature (1994 field data, courtesy of BODC)

model, from January to September. During the winter, the water column is homogeneous because heat exchange through the atmosphere/water interface is not strong enough to develop a vertical gradient. In the spring, the sun heats the surface water, which increases the stratification of the water column. As we shall see, the strong summer stratification has deep biological implications; the pycnocline associated with the thermocline acts like a nutrient barrier and, as nutrients are depleted in superficial water, a nutricline develops (figure 4).

Some generic assumptions were made in order to run the biogeochemical model. The particulate organic matter (POM) decomposition is neglected; POM sinking rate is about 100 m day^{-1} (Parsons, Takahashi and Hargrave, 1995), and decomposition is assumed to take place below the photic layer, not immediately available to photosynthetic producers. Nitrification (transformation of ammonia into nitrate) is tuned to zero, since the rate of consumption of ammonia by primary producers is fast enough to make this process negligible. These assumptions are implicitly made in the new and regenerated production analysis as proposed by Eppley and Peterson (1979), still a common practice (e.g. Harrison, Harris and Irwin, 1996; Joint, Rees and Pomroy, 1996; Elskens, Dehairs and Goeyens, 1996).

The annual planktonic primary production evolution at Goban Spur/La Chappele is typical of temperate oligotrophic waters. At middle latitudes, sunlight is not strong enough to provide maximal potential primary production throughout the year, leading to strong seasonal fluctuations (Wollast, 1997).

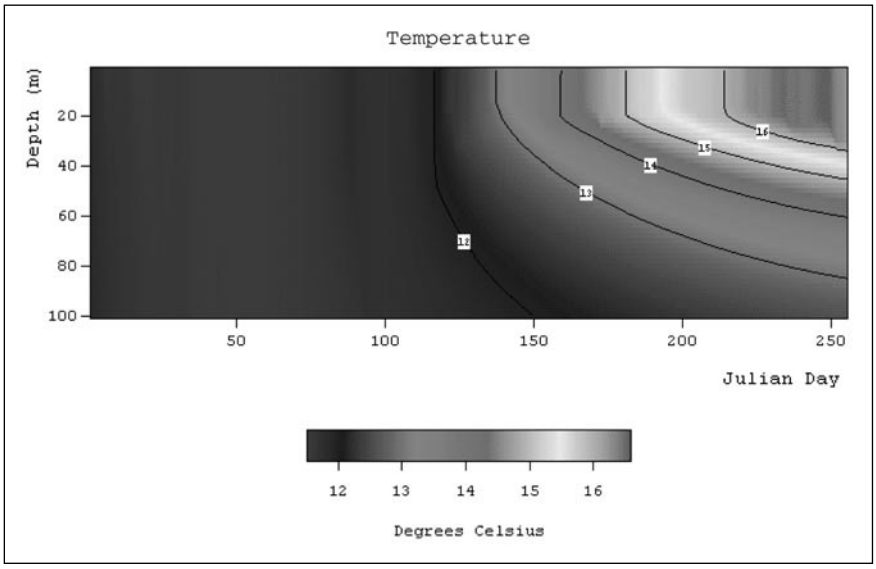

Figure 3. Temperature range from January to September. In winter the water column is homogeneous, evolving into a strong stratification situation in summer

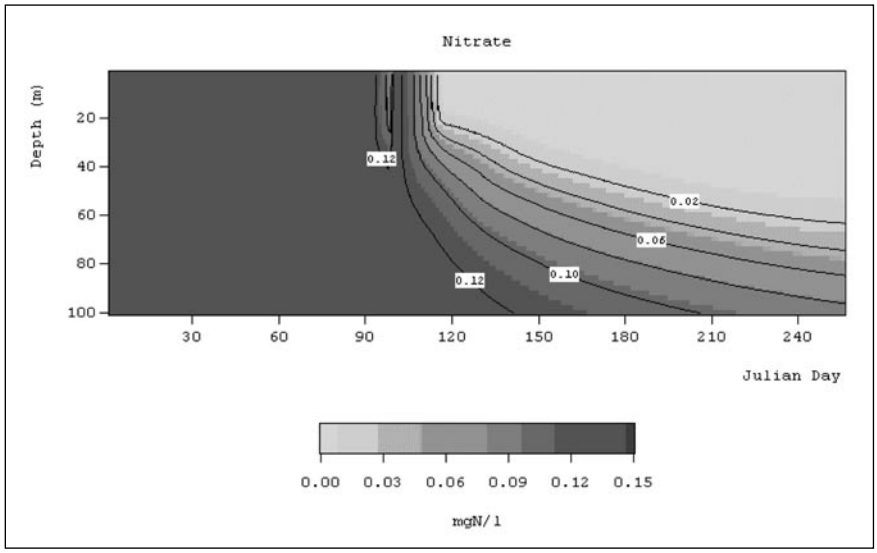

Figure 4. Primary producers' concentration, from January to September

Following the low primary-production level during winter, the spring bloom appears. The mechanism of the spring bloom (Cushing, 1989; Mann, 1993) starts with the turbulent mixing of the water column bringing nutrients to the surface. In the spring, the increase of temperature due to solar radiation leads to the formation of the mixed layer. When the depth of the mixed layer equals the compensation depth (roughly the depth where the light is 1 % of surface light; respiration and production above the compensation depth balance each other), there are conditions for the spring bloom to begin. The strong seasonal thermocline is a barrier to the diffusion of nutrients from rich deep waters. Diatoms, being an opportunistic species (Valiela, 1995), develop in a short period of time and deplete nutrients in the mixed layer. Afterwards, a subsuperficial flagellate-dominated maximum appears at the thermocline. In autumn, as the days get shorter, the thermocline deepens and conditions favourable to a second bloom may appear.

The model was applied to the period from January to September, simulating the spring bloom and the stratified water column of the summer oligotrophic production period (figure 5 shows the autotrophic producers' concentration). The chlorophyll subsuperficial maximum (CSM) develops at the end of the spring bloom, and intensifies during the summer.

The stratified conditions of the summer water column inhibit the flux of nutrients from the rich deep water to the depleted surface water; the sum-

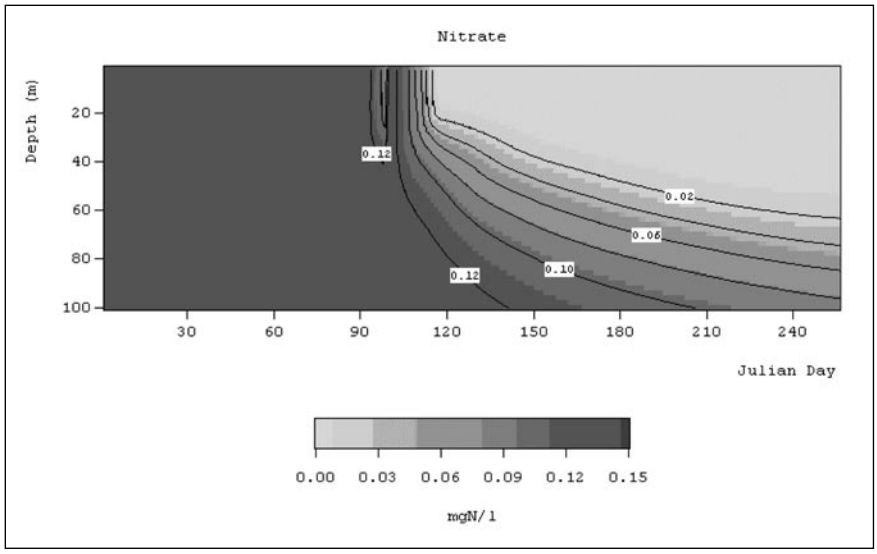

Figure 5. Nitrate concentration from January to September

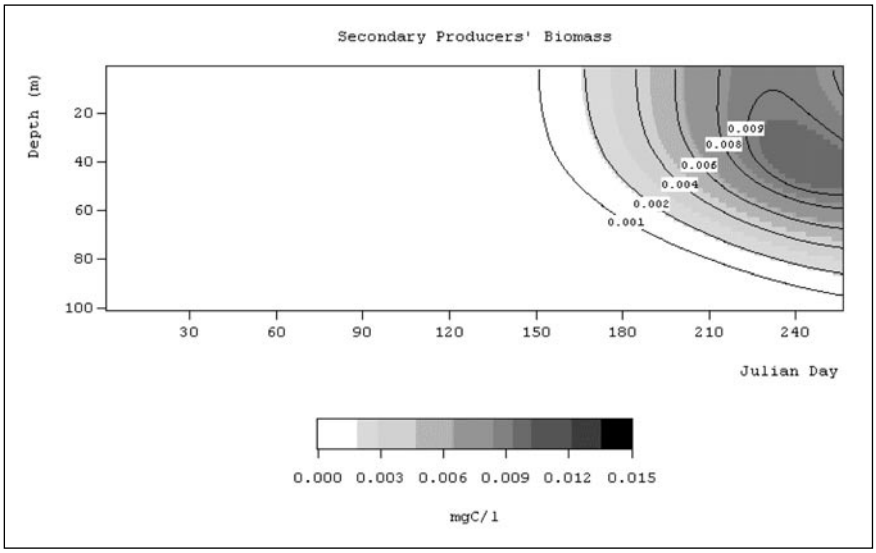

Figure 6. Secondary producers' concentration, from January to September

mer nutricline is visible in figure 4, showing nitrate concentration.

The secondary producers' biomass increases with a time lag from the primary producers' bloom. In fact, in the oligotrophic North Atlantic, the growth of heterotrophic producer populations responds to the enhanced autotrophs' enhanced biomass and not to their higher rate (figure 6).

The spring bloom is subsidised by nitrate; i.e. new production dominates. As the spring bloom ends, with the depletion of nitrate in the mixed layer, 'regenerated production' gains importance in the overall budget. Accordingly, the plot of f-ratio (new production/total production, figure 7) increases during the spring bloom and reaches its lowest values during the summer.

To assert the influence of grazing pressure over primary producers' concentration, the model was run without secondary producers (figure 8). Below, in the Discussion section, a comparison between the results with and without grazers is presented.

Lagrangian approach

In the Lagrangian approach all the assumptions made to run the biochemical model are the same as the ones used in the Eulerian approach. The 1-D hydrodynamic model used is also the same. The only difference between these two approaches is how transport of the biochemical properties is computed. In the Eulerian approach, a simple fi-

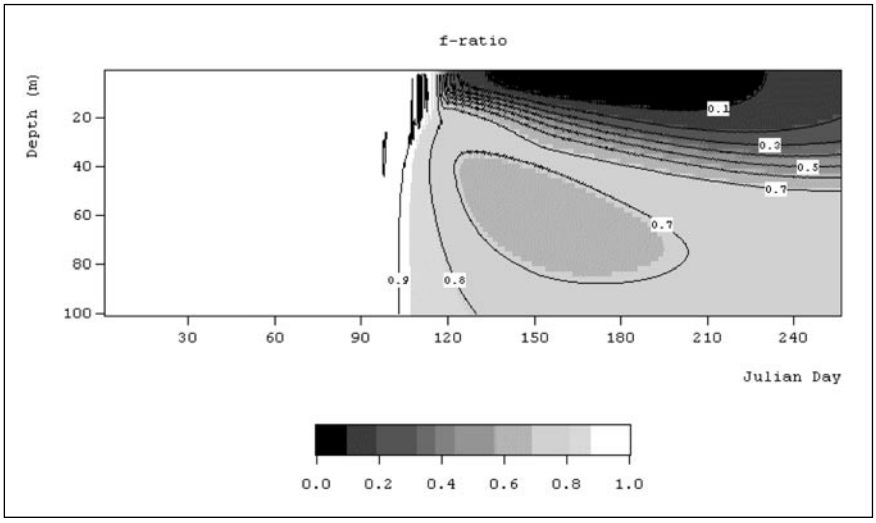

Figure 7. f-ratio, from January to September

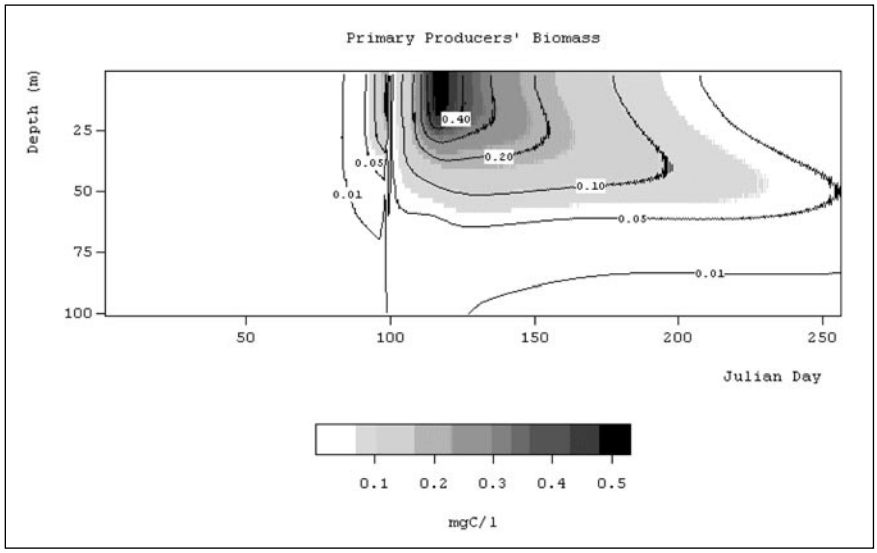

Figure 8. Primary producers' concentration, model run without secondary producers, from January to September

nite-difference method is used to solve the transport equation, whereas in the Lagrangian approach a particle-tracking method is used. This method solves the transport equation to control the volumes moving with the flow. In this particular study case, only vertical diffusion forced the properties transport. To simulate vertical diffusion in the ocean, the particle-tracking model needs vertical turbulent velocity standard deviation (figure 9) and mixing lengths (figures 10 and 11). The mixing lengths are a direct result of the 1-D hydrodynamic model. The turbulent velocity can be computed from the turbulent kinetic energy that is also a direct result of the 1-D hydrodynamic model. Figures 9, 10 and 11 show very clearly the evolution of the ocean's mixed layer. One particular characteristic of these results is the sharp narrowing of the mixed layer in the beginning of spring. This is the forcing mechanism of the spring bloom.

To understand the effect of the brisk water stratification in the spring bloom, two water masses were followed throughout a whole year. Both water masses were emitted near the surface in 1994/1/1 (figure 12). Due to the stochastic nature of the process, they have different trajectories. The first one, which we will call particle 1, was only able to stay in the mixed layer until Julian day 110 (approximately). The other one, particle 2, also stayed in the mixed layer until Julian day 115 (approximately) but around the Julian day 150 it was able to return. It is interesting to see how the trajectory of water masses influences their primary production

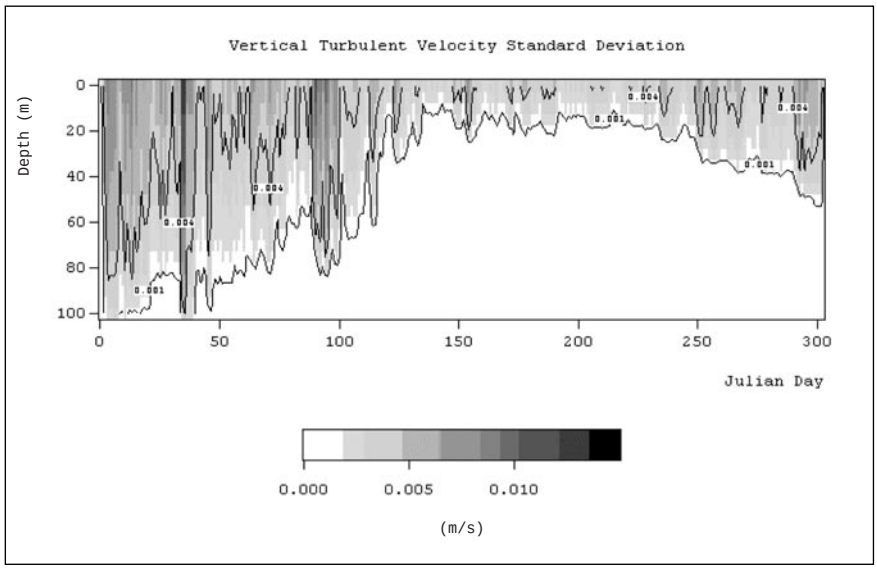

Figure 9. Evolution of the vertical turbulent velocity standard deviation between depth of 0-100 m during 300 days

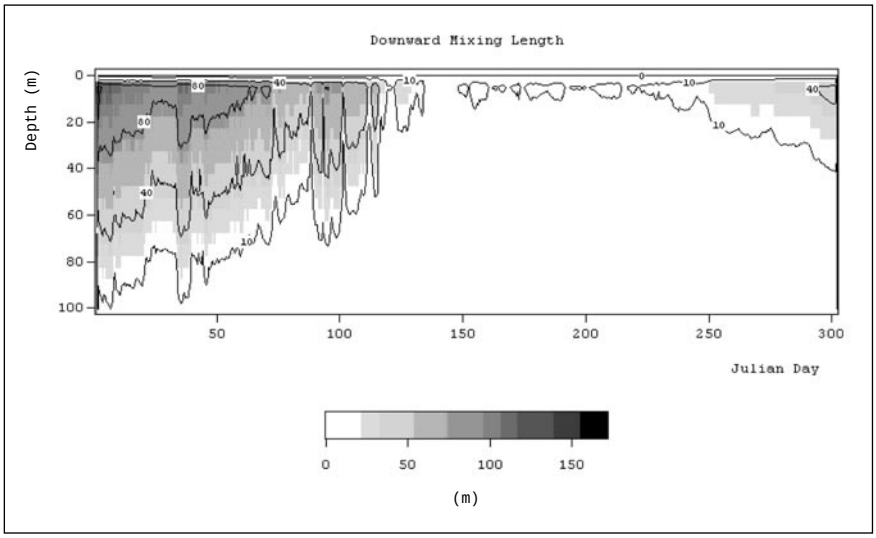

Figure 10. Evolution of the downward mixing length between depth of 0-100 m during 300 days

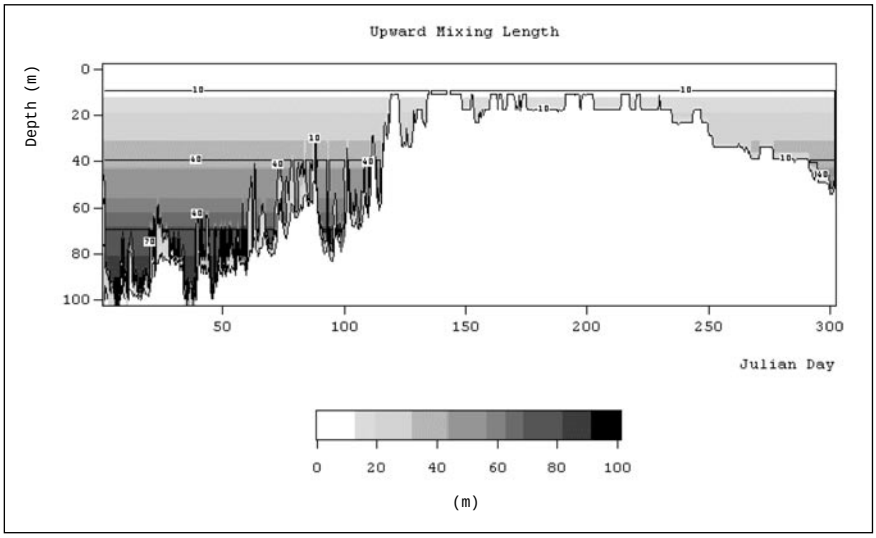

Figure 11. Evolution of the upward mixing length between depth of 0-100 m during 300 days

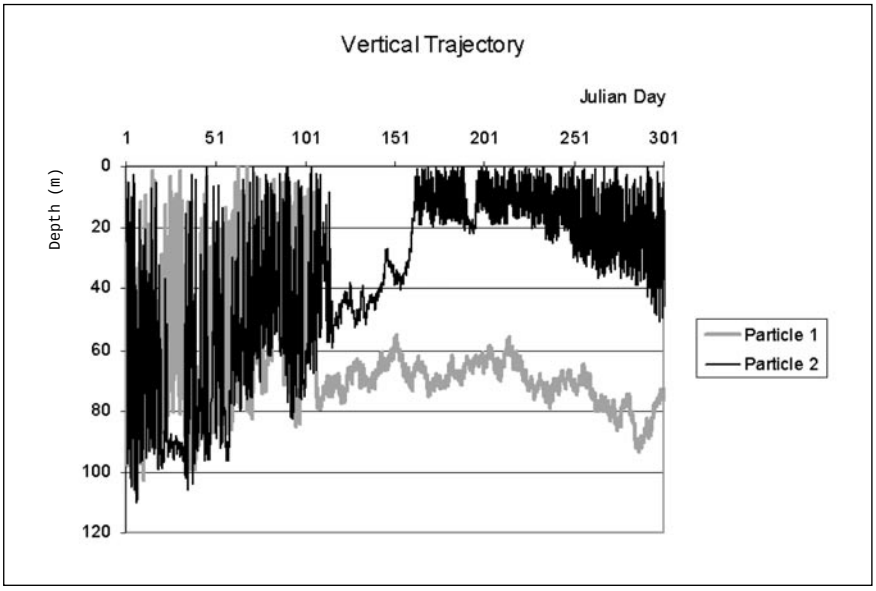

Figure 12. Vertical trajectory of two particles emitted near the surface on 1994/1/1

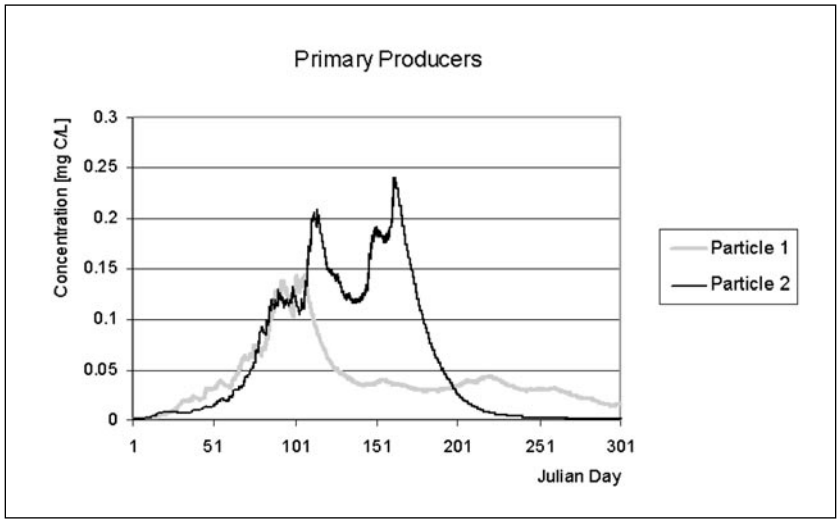

Figure 13. Evolution of two particles' phytoplankton concentrations during 300 days

(figure 13). The particle 1 primary producers' concentration grows until it leaves the mixed layer, when its concentration decreases very rapidly until it stabilises around a value of 0.04 mg C/l. The particle 2 primary producers' concentration has two peaks, the first one corresponding to the water mass leaving the mixed layer, and the second one corresponding to the particle return to the mixed layer followed by the depletion of the nitrates (figure 14).

A run where 2 000 particles were followed was also performed, with the aim of comparing the results of the Lagrangian approach with the Dulerian approach. The particles were evenly emitted on Julian day 1 at depths of 0-100 m. Their trajectory was followed during 250 days. The results were interpolated to a Eulerian grid with 1-m step in the vertical. Figures 15, 16 and 17 show the results of primary producers' biomass and nitrate concentrations, and secondary producers' biomass concentrations during 250 Julian days, a depths between 0-100 m. We can conclude from a general analysis that both approaches give similar results. One of the main differences is that in the Lagrangian approach, the spring bloom gradients are softer.

Biochemical 3-D hydrodynamic results

Over the last 4 years a 3-D baroclinic model (Santos, 1995) has been used to simulate the hydrodynamic flow field along the Iberian Continental Shelf (Coelho *et al.*, 1994). The model uses the Boussinesq, hydrostatic and beta plane approximations and a mixing length turbulent closure similar to the one described in Nihoul (1984). The equa-

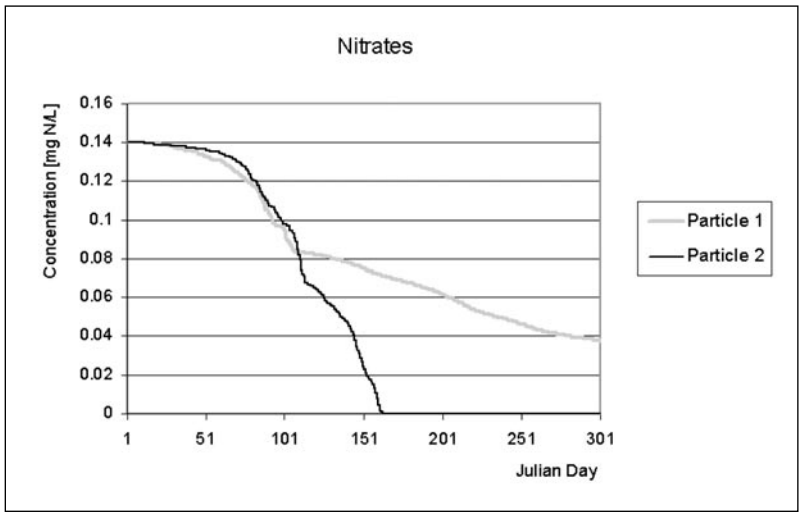

Figure 14. Evolution of two particles' nitrate concentrations during 300 days

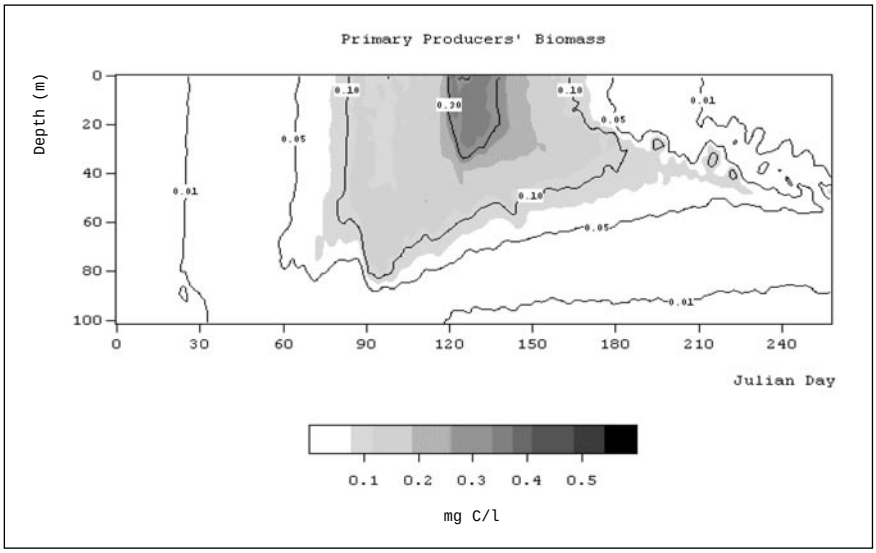

Figure 15. Evolution of the phytoplankton concentration during 250 days between depth of 0-100 m

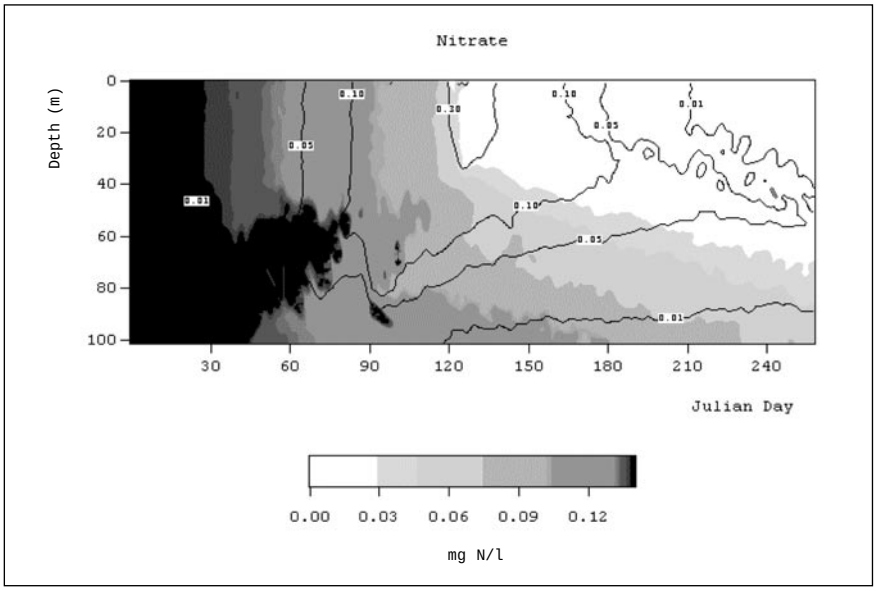

Figure 16. Evolution of nitrate concentration during 250 days

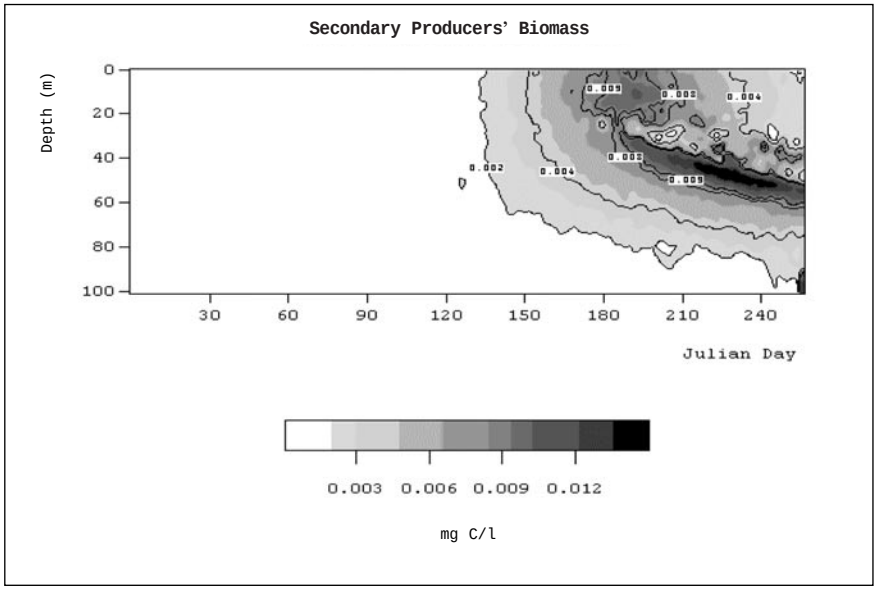

Figure 17. Evolution of the zooplankton concentration during 250 days

tions of continuity, momentum, salt and heat conservation are solved with a double sigma co-ordinate, imposing a radiation condition at the open boundaries. The numerical method used is a finite-differences one, with an implicit discretisation of the terms imposing more stability limitations (free surface waves, vertical transport and bottom friction).

The model has been forced with climatologic density field and real-wind fields. In the future, forcing due to tides will also be considered. The model domain is 30°60° N and 25°-8° E, although only results in the area 43°-53° N and 20°-0° W will be presented. The study area includes the Bay of Biscay, La Chapelle Bank, the Goban Spur and the Celtic Sea.

This work has been carried out within the framework of the European OMEX programme. The main goal of this programme is to determine physically-controlled advective and diffusive transports and fluxes in varied shelf-edge contexts, and thence to devise an adequate representation of the ocean and shelf-boundary conditions for prognostic (ultimately 3-D numerical) models. The results show the upwelling areas along the coast and the slope, and allow visualisation of the transport along and across the slope. One of the final products of this project were four stationary 3-D velocity fields that characterised well the flow tendency in spring, summer, autumn and winter. Only climatological density fields forced these velocity fields.

Our main objective in the present paper is to show that a 3-D particle-tracking model coupled with a 3-D hydrodynamic model (with a turbulence closure model similar to the one described earlier) and a biochemical model can be an excellent tool to quantify exchanges between the continental shelf and the deep ocean. The spring bloom results presented have shown that the Lagrangian approach give similar results to the Eulerian approach. If we want to quantify the exchanges along the slope, it is necessary to take into account not only the vertical mixing, but also the horizontal and vertical (upwelling and downwelling) advections. In this case, a Lagrangian transport model is more useful because it does not present the problems of numerical diffusion associated with the resolution of the advective term, which happens when the Eulerian approach is used.

To illustrate the model coupling described in this paper, a run was made for 20 days starting at the beginning of April. Between depths of 60 and 80 m, 40 000 particles were emitted. Figures 18 and 19 show the evolution of the particles' position, showing some strong upwelling movements on the Galiza coast and along the slope between La Chapelle Bank and the Goban Spur. These results are consistent with remote sensing results (SST images) presented by Miller *et al.* (1996). The phytoplankton concentration results (figures 20 and 21) are also in good agreement with remote sensing data (CZCS images) in Miller *et al.* (1996).

These model results were not obtained with a complete model coupling. In a first stage, a spring climatologic density field forced the 3-D hydrodynamic model until a stationary situation was obtained. Finally, the 3-D particle-tracking model run

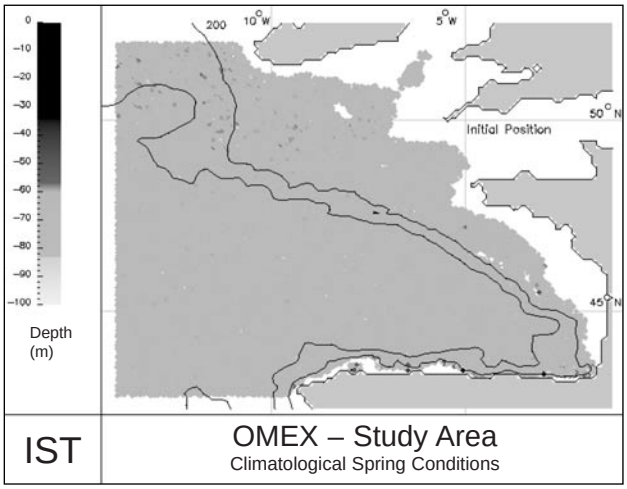

Figure 18. Particles (or tracers) emitted between depth of 60-80 m. The colour represents the depth of each tracer. Initial position

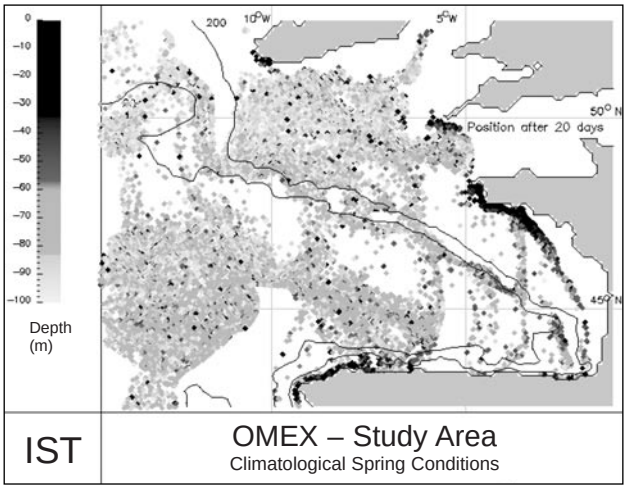

Figure 19. Particles (or tracers) emitted between depths of 60-80 m. The colour represents the depth of each tracer. Position after 20 days

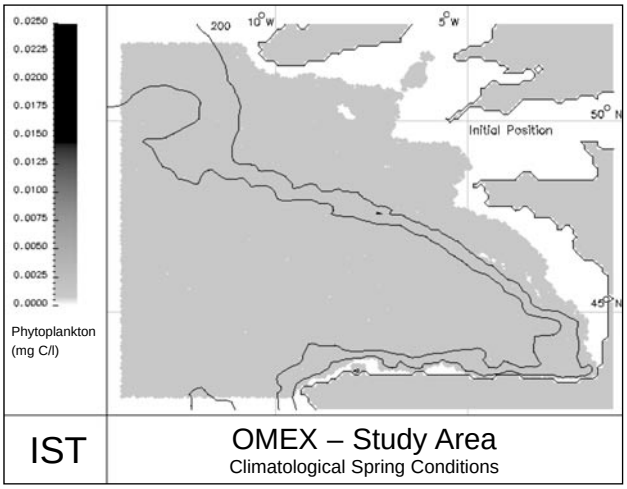

Figure 20. Particles (or tracers) emitted between depth of 60-80 m. The colour represents the phytoplankton concentration of each tracer. Initial position

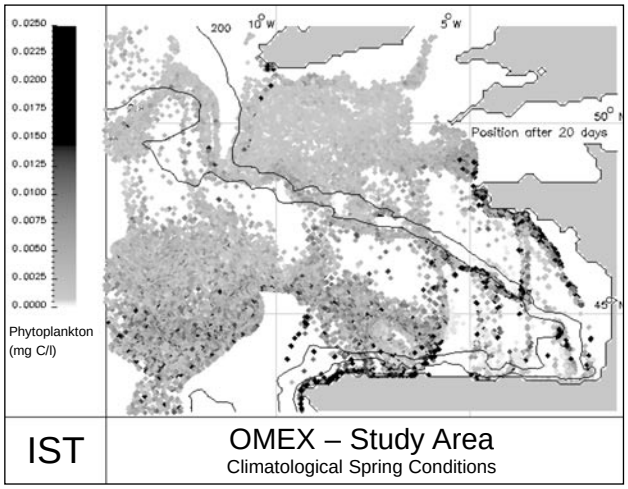

Figure 21. Particles (or tracers) emitted between depths of 60-80 m. The colour represents the phytoplankton concentration of each tracer. Position after 20 days

20 days coupled with the 1-D turbulence model and the biochemical model, using the 3-D stationary velocity field to compute the advection transport.

DISCUSSION

The Goban Spur/La Chapelle primary-production seasonal cycle follows the temperate waters trend. The periodic presence of the CSM is an important feature of these ecosystems, whose correct quantification and simulation is a major challenge. The main source of global primary production information are currently satellite images, which merely give direct information on superficial chlorophyll concentration, say 0.1 m deep, and from which we must be able to predict the depth- integrated production. On the other hand, several physical and biological processes leading to the formation and maintenance of the CSM have been proposed; numerical models able to reproduce the CSM are a powerful tool to test and study these hypotheses.

Model results presented in section 'Biochemical 1-D hydrodynamic model' show good agreement with field data (Anon., 1996). There was a small spring bloom at the beginning of April but, probably due to excessive wind mixing, it was interrupted and the spring bloom started in the second half of April. Due to the primary production increase, a nitracline appeared in May (figure 5) and remained throughout the simulation (when days get shorter in the autumn, water-column stratification disappears, causing the disappearence of the nitracline). Secondary production shows a time lag with primary production, which is in accordance with other studies made in the Atlantic Ocean's mild oligotrophic waters (there is no field data for heterotrophs in the study area to validate the model).

As noted above, diatoms form the bulk of the spring bloom, being replaced by flagellates when the water column stratifies and CSM develops. Diatoms float passively, depending on the presence of turbulence to maintain themselves in the photic zone; during turbulence-free periods they sink and may get out of the euphotic layer. Dead diatom skeletons are heavy silicate structures that sink quickly into deep water. Large diatom populations usually lead to enhanced ecosystem export of organic material. In contrast, flagellates are able to swim, and can actively search for food and keep themselves within the euphotic zone (Cushing, 1989). Although several authors divide autotrophs into different populations in their models (e.g. Moisan and Hofmann, 1996) or include a primary producers' sinking rate (e.g. Anon., 1987; Rodrigues, 1997), the present model simulates the CSM without introducing a primary producers' sinking rate. Particulate organic matter, which includes dead plankton, was assumed to sink without decomposition in the euphotic zone.

The influence of secondary producers' grazing pressure on primary producers' populations may be an important factor in the development of the

CSM. According to Roman *et al.*, (1986, in Moisan and Hofmann, 1996), grazing serves to remove phytoplankton biomass in the upper water column and shifts absolute production to depth. This is not confirmed by our model result. Comparing figure 4 with figure 8, it seems noteworthy that the maximum chlorophyll depth does not change, and in the presence of grazers the stratified conditions' CSM is smaller. The overall impact of grazing on primary production during the spring bloom at Goban Spur is small. This is in agreement with former studies in the Atlantic Ocean's oligotrophic temperate waters that indicate a bottom-up control of secondary producers during the spring bloom, and breeding of zooplankton cannot start until an increase in primary production has occurred (Parsons, Takahashi and Hargrave, 1995).

The coupling of a 3-D hydrodynamic model with a 3-D particle-tracking model and a biochemical model proves to be a very powerful tool to quantify the exchanges between the deep ocean and the continental shelf. Our results show a very good agreement with the SST and CZCS images for springtime (Miller *et al.*, 1996; Groom *et al.*, in preparation). However, it is very difficult to calibrate a model of this type, considering the large scales involved. Systematic work on calibration will be done in the future, based not only on satellite images, but also on field data. A full coupling is also planned; i.e. the 3-D hydrodynamic model will be running at the same time of the biochemical and particle-tracking models.

REFERENCES

Allen, C. M. 1982. Numerical simulation of contaminant dispersion in estuary flows. *Proceedings of the Royal Society of London* A 381: 179-194.

Anon. 1987. *QUAL2: The Enhanced Stream Water Quality Models. Documentation and User Model.* Environmental Protection Agency. Athens, Georgia: 189 pp.

Anon. 1996. OMEX: Ocean Margin Exchange, contract number MAS2-CT93-0069, Final Report, Subproject D - *Biogeochemical Cycles*, Université Libre de Bruxelles, Proudman Oceanographic Laboratory, Norwegian College of Fishery Science, Plymouth Marine Laboratory, Netherlands Institute for Sea Research, RISØ National Laboratory: 591 pp.

Bork, I. and E. Maier-Reimer. 1978. On the spreading of power plant cooling water in a tidal river applied to the River Elbe. *Advances in Water Resources* 1 (3): 161-168.

Bougeault, P and J. C. André. 1986. On the stability of the third order turbulence closure for modelling of the stratocumulus-topped boundary layer. *J. Atmos. Sci.* 43: 1574-1581.

Bougeault, P. and P. Lacarrère. 1989. Parameterisation of orography-induced turbulence in a meso-beta scale model. *Mon. Weather Rev.* 117: 1872-1890.

Bryan, F. and M. D. Cox. 1972. An approximate equation of state for numerical models of ocean circulation. *J. Phys. Oceanogr.* 17: 970-985.

Coelho, H. 1996. *Modelação Numérica da Turbulência Oceânica*. Ms.C. thesis. Instituto Superior Técnico, Universidade Técnica de Lisboa, Lisboa: 89 pp.

Coelho, H., A. Santos, T. Rosa and R. Neves. 1994. Upwelling in the Iberian Coast. Modelling of Coastal and Estuarine Processes. In: *Modelling of Coastal and Estuarine Processes.* F. J. Seabra and A. Temperville (eds.): Special issue of *Estudos de Engenharia Civil* 6: 235-243. Coimbra, Portugal.

Collins, C. D. 1980. Formulation and validation of a mathematical model of phytoplankton growth. *Ecology* 61: 639-649.

Collins, C. D. and R. A. Park. 1989. Primary productivity. In: *Mathematic Submodels in Water Quality Systems*: 299-330. Elsevier Science Publishers, Amsterdam.

Cushing, D. H. 1989. A difference in structure between ecosystems in strongly stratified waters and in those that are only weakly stratified. *J. Plankton Res.* 11 (1): 1-13.

Dippner, J. 1993. A Lagrangian model of phytoplankton growth dynamics for the Northern Adriatic Sea. *Continental Shelf Research* 13 (2/3): 331-353.

Elskens, M., F. Dehairs and L. Goeyens. 1996. Variable Nitrate Contributions in the Uptake by Phytoplankton of an Ocean Margin Environment. Ocean Margin EXchange, contract number MAS2-CT93-0069, Final Report, Subproject D - *Biogeochemical Cycles*, Université Libre de Bruxelles, Proudman Oceanographic Laboratory, Norwegian College of Fishery Science, Plymouth Marine Laboratory, Netherlands Institute for Sea Research, RISØ National Laboratory: 389-411.

Eppley, R. W. and B. J. Peterson. 1979. Particulate organic matter flux and planktonic new production in the deep ocean. *Nature* 282: 677-680.

Galperin, B., H. Kanthal, S. Hassid and A. Rosati. 1988. A quasi-equlibrium turbulent energy model for geophysical flows. *J. Atmos. Sci.* 45: 113-132.

Gaspar, P., Y. Grégoris and L. M. Lefevre. 1990. A simple eddy kinetic energy model for simulations of the oceanic vertical mixing: Tests at Station Papa and Long-Term Upper Ocean Study site. *J. Geophys. Res.* 95 (16): 179-193.

Gregg, M. C., H. Peters, J. C. Wesson, N. S. Oakey and T. J. Shay. 1985. Intensive measurements of turbulence and shear in the equatorial undercurrent. *Nature* 318: 140-144.

Harrison, W. G., L. R. Harris and B. D. Irwin. 1996. The kinetics of nitrogen utilization in the oceanic mixed layer: Nitrate and ammonium interactions at nanomolar concentrations. *Limnology and Oceanography* 41 (1): 16-32.

Huthnance, J. M., J. I. Allen, A. M. Davies, D. J. Hydes, I. D. James, J. E. Jones, G. E. Millward, D. Prandle, R. Proctor,

D. A. Purdie, P. J. Statham, P. B. Tett, S. Thomson and R. G. Wood. 1993. Towards water quality models. *Philos. T. Roy. Soc. Lon.* A343: 569-584.

Isaacs, J. D. 1973. Potential trophic biomasses and trace-substance concentrations in unstructured marine food webs. *Mar. Biol.* 22: 97-104.

Ivlev, V. S. 1945. The biological productivity of waters. *Uspekhi Soremenoi Biologii* 19 (1): 98-120.

Joint, I., A. Rees and A. Pomroy. 1996. Primary and New Production. Ocean Margin EXchange, contract number MAS2-CT93-0069, Final Report, Subproject D - *Biogeochemical Cycles*, Université Libre de Bruxelles, Proudman Oceanographic Laboratory, Norwegian College of Fishery Science, Plymouth Marine Laboratory, Netherlands Institute for Sea Research, RISØ National Laboratory: 337-370.

Kelsey, A., C. M. Allen, K. J. Beven and P. A. Carling. 1994. Particle Tracking Model of Sediment Transport. In: *Mixing and Transport in the Environment*. K. J. Beven, P. C. Chatwin and J. H. Millbank (eds.): 419-442. John Wiley & Sons Ltd, New York.

Large, W. G. and S. Pond. 1981. Open ocean momentum flux measurements in moderate to strong winds. *J. Phys. Oceanogr.* 11: 324-336.

Large, W. G. and S. Pond. 1982. Sensible and latent heat flux measurements over the ocean. *J. Phys. Oceanogr.* 12: 464-482.

Leitão, P. 1997. *Modelo de Dispersão Lagrangeano Tridimensional*. Master's thesis, Universidade Técnica de Lisboa. Instituto Superior Técnico. Lisbon: 134 pp.

Mann, K. H. 1988. Towards Preditive Models for Coastal Marine Ecossystems. In: *Concepts of Ecossystem Ecology*. L. R. Pomeroy and J. J. Alberts (eds.): 291-316. 1st ed. Springer-Verlag, New York.

Mann, K. H. 1993. Physical oceanography, food chains, and fish stocks: a review. *J. Mar. Sci.* 50: 105-119.

Mansur, L. and D. M. Price. 1992. Oil-RW: A mathematical model for predicting oil spills trajectory and weathering. Hydraulic and Environmental Modelling: Coastal Waters. In: *Proceedings of the Second International Conference on Hydraulic and Environmental Modelling of Coastal, Estuarine and River Waters*. R. A. Falconer, S. N. Chandler-Wilde and S. Q. Liu (eds.) 1: 201-212, University of Bradford, UK.

Mellor, G. L. and T. Yamada. 1982. Development of a turbulence closure model for geophysical fluid problems. *Rev. Geophys.* 20: 851-875.

Miller, P., S. Groom, A. McManus, J. Selley, J. Woolfenden, J. Blewett and E. Osborne. 1996. Remote sensing activities in OMEX. European project: Ocean Margin Exchange OMEX I - Final Report: 52 pp.

Moisan, J. R. and E. E. Hofmann. 1996. Modeling nutrient and plankton processes in the California Coastal Transition Zone 1. A time- and depth-dependent model. *J. Geophys. Res.* 101 (C10): 22647-22676.

Monteiro, A. J., R. J. Neves and E. R. Sousa. 1992. Modelling transport and dispersion of effluent outfalls. *Water Science and Technology WSTED4* 25 (9): 143-154.

Neves, R. J. J. 1985. *Étude Experimentale et Modélisation des Circulations Trasitoire et Résiduelle dans l'Estuaire du Sado*. Doctoral thesis. Univ. Liège: 371 pp.

Neves, R. J. J. and F. A. Martins. 1996. Modelação Lagrangeana dos Processos de Transporte na Ria Formosa. In: 5ª Conferência Nacional Sobre a Qualidade do Ambiente. C. Borrego, C. Coelho, L. Arroja, C. Boia, E. Figueiredo: Volume 2 pp: 1985-1996, Comissão de Coordenação da Região Centro (CCRC), University of Aveiro, Aveiro, Portugal.

Nihoul, J. C. J. 1984. A three-dimensional general marine circulation model in a remote sensing perspective. *Annales Geophysicae* 2 (4): 433-442.

Odum, E. P. 1971. Fundamentals of Ecology. 3rd Ed. W. B. Saunders Company, Philadelphia: 574 pp. Modeling, Troy, NewYork.

Parsons, T. R., R. J. Lebrasseur and J. D. Fulton. 1967. Some observations on the cell size and concentration of phytoplankton blooms. *Journal Ocean. Soc. Japan* 23 (1): 10-17.

Parsons, T. R., M. Takahashi and B. Hargrave. 1995. Biological Oceanographic Processes. 3rd ed. Butterworth Heinemann, Oxford: 330 pp.

Rodgers, P. and D. Salisbury. 1981. Water quality modeling of Lake Michigan and consideration of the anomalous ice cover of 1976-77. *J. Great Lakes Res.* 7 (4): 467-480.

Rodrigues, V. 1997. Modelação Ecológica e da Qualidade da Água em Zonas Costeiras Utilizando a Aproximação Lagrangeana. Ms.C. thesis, Instituto Superior Técnico, Universidade Técnica de Lisboa, Lisboa, 110 pp.

Rodrigues, V., R. J. J. Neves and R. Miranda. 1996. Modelação ecológica e da qualidade da água em zonas costeiras. In: *5.ª Conferência Nacional Sobre a Qualidade do Ambiente*. C. Borrego, C. Coelho, L. Arroja, C. Boia and E. Figueiredo (eds.) 2: 2005-2023. Comissão de Coordenação da Região Centro (CCRC), University of Aveiro, Aveiro, Portugal.

Santos, A. J. 1995. Modelo Hidrodinâmico Tridimensional de Circulação Oceânica e Estuarina. Ph.D. Instituto Superior Técnico, Univ. Técnica de Lisboa: 273 pp.

Scavia, D. 1980. An ecological model of Lake Ontario. *Ecological Modelling* 8: 49-78.

Scavia, D., C. W. Boylen, R. B. Sheldon and R. A. Park. 1976. An ecological model for Lake Ontario: Model formulation, calibration, and preliminary evaluation. NOAA Technical Report ERL 371-GLERL 12, Great Lakes Environmental Research Laboratory, Ann Arbor, MI (PB-262-412/0GI): 63 pp.

Shiau, B. 1991. Computer modelling of oil pollutants transport on the water. *Computer Modelling in Ocean Engineering* 91: 467-475.

Steele, J. H. 1962. Environmental control of photosynthesis in the sea. *Limnology and Oceanography* 7: 137-150.

Thornton, K. W. and A. S. Lessen. 1978. A temperature algorithm for modifying biological rates. *T. Am. Fish. Soc.* 107 (2): 284-287.

Valiela, I. 1995. *Marine Ecological Processes*. 2nd ed. Springer Verlag, Marine Ecological Processes. 2nd ed. Springer Verlag, New York: 686 pp.

Wollast, R. 1997. Evaluation and comparison of the global carbon cycle in the coastal zone and in the open ocean.

In: *The Sea - The Global Coastal Ocean, Vol. 10, Ideas and Observations on Progress in the Study of the Seas*. K. H. Brink and A. R. Robinson (eds.). John Wiley & Sons Ltd. New York: 230 pp.

Woods, J. D. and R. Onken. 1982. Diurnal variation and primary production in the ocean. Preliminary results of a Langrangian ensemble model. *J. Plankton Res.* 4 (3): 735-756.